

## Effect of Wing flexibility on Dragonfly Hover Flight.

V. Naidu, J. Young and J.C.S. Lai

School of Engineering and Information Technology  
 University of New South Wales,ADFA, ACT 2600, Australia

### Abstract

The role of wing flexibility in tandem wings during the hover flight at phase  $180^\circ$  was investigated using Fluid Structure Interaction (FSI) simulations. The wing shapes were that of the dragonfly species *Aeshna Juncea* and the flexible wing models displayed wing stiffnesses as found in the real wings. Wing flexibility enhanced the lift generated by both the tandem wings, with the forewing and the hindwing generating 10% and 17% more lift respectively, as compared to the rigid wings.

### Nomenclature

$E$	=	Young's modulus.
$\nu$	=	Poisson's ratio.
$f$	=	Flapping frequency.
$\beta$	=	Stroke plane angle.
$\alpha_u$	=	Upstroke pitch angle.
$\alpha_d$	=	Downstroke pitch angle.
$\bar{c}_f$	=	Forewing mean chord length.
$\rho$	=	Density.
$T$	=	Flapping period.

### Introduction

Insect aerodynamics has generated substantial research interest in the past few decades, as their flight techniques may inspire the design of Micro Air Vehicles (MAVs). These MAVs can be used for surveillance purposes, search and rescue operations or for applications where conventional aircraft cannot be deployed. Insects are capable of flying in different speeds, ranging from a Reynolds number of 10 to  $10^5$ . They display different aerodynamic mechanisms like clap and fling, wing rotation, delayed stall of the leading edge, wake capture, etc. [13].

Most insects have one pair of wings; however insects like the dragonfly and the locust have two pairs of wings arranged in tandem position. This arrangement of the wings leads to complex aerodynamic interactions between the two wing pairs, since the hind wing is in the wake generated by the fore wing. Dragonflies flap their wing pairs in-phase i.e. both wings flap in synchronisation or flap out-of-phase i.e. one followed by the other, depending upon the requirements of take-off, hover, manoeuvre and forward flight [1, 2].

A number of experimental studies [9, 8, 16, 7] and numerical investigations [14, 15, 17, 6] under different flight modes have been carried out to understand these complex flow interactions between tandem flapping wings. However, most tandem wing studies have been confined to rigid wings, unlike the highly flexible dragonfly wings in nature, with spanwise and chordwise varying flexibility [4]. Flexibility in the wing, results in an in-flight deformation of the wing, which alters the aerodynamic performance as compared to the rigid wings.

Investigation on locust wings shows that flexibility maintains attached flow and helps in improving the flight efficiency [18]. A comparative study between a single pair of flexible and rigid dragonfly wings using fluid structure interaction (FSI) shows

that a rigid wing requires 34% more peak power than the flexible wing [6]. A flexible tandem wing study using a rectangular wing shape [16], shows that flexibility improves lift efficiency in both the wings. Hence, it is important to investigate the role of wing flexibility in dragonfly flight.

In this study, the hovering flight mode with phase  $180^\circ$  is considered and the wing kinematics is the same as in the study of Young et al [17]. The wings are simplified as a flat plate without any corrugations and the wing material properties are chosen to mimic the varying spanwise and chordwise stiffness as found in the real wing [4]. The flexible wing simulations are carried out using two-way Fluid Structure Interaction (FSI) and their performance is compared with the rigid tandem wings.

### Wing Model

The tandem wings shapes are that of the dragonfly species *Aeshna Juncea*, taken from [11]. The dragonfly wings are lightweight, highly corrugated structures [12], composed of a network of veins and membranes. Another unique feature of the dragonfly wings is the presence of the *pterostigma* near the wing tip, which is nearly 9% and 16% of the forewing and the hindwing mass respectively [11].

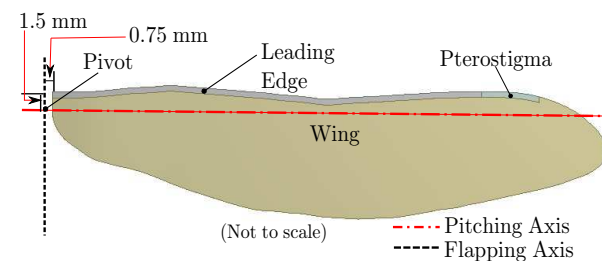


Figure 1. Dragonfly forewing model.

In our model, for simplicity the wings are assumed to be made up of flat surfaces, without any corrugations. Figure 1, shows the schematic of the forewing used in the FSI simulations, which is composed of the the main *wing*, the *leading edge* and the *pterostigma* near the wing tip. The spanwise stiffness of a dragonfly wing is higher than the chordwise stiffness by nearly 2 orders of magnitude [4]. To accommodate this anisotropy in the material behaviour, an *orthotropic* material is used for the main wing by using different Young's modulus ( $E$ ) for the span and the chord directions. The material properties in the thickness direction are assumed to be the same as that of the spanwise direction. To accommodate spanwise stiffness variation, thickness is reduced along the span from the wing root to the wing tip.

The leading edge of the wing and the pterostigma are assumed to be made of isotropic material. The Poisson's ratio for all the three components is assumed to be 0.3. Table 1 summarises the wing material properties. The densities of the components are appropriately chosen to match the mass of the wing, the pterostigma and also to match the mean centre of mass location along the chord as reported in [11].

Component	Material	$E$ (GPa)	$\rho$ ( $kg/m^3$ )
Wing	Orthotropic	14 (Spanwise)	74
		0.03 (Chordwise)	
		14 (Thickness)	
Pterostigma	Isotropic	30	3256
Leading Edge	Isotropic	30	1000

Table 1. Forewing material properties.

Using the static bending test method to estimate the stiffness of the wings as described in [4], the forewing stiffness at the wing root and the leading edge was estimated respectively as  $1.8e^{-4}Nm^2$  and  $6.2e^{-7}Nm^2$ , within the range of the real wings. The first mode frequency of the forewing was found by modal analysis to be  $171Hz$ , which is close to that estimated in a real forewing [3]. The same material properties were used for the hindwing with densities of  $68,1841.5$  and  $1325 kg/m^3$  for the wing, the pterostigma and the leading edge, respectively. The hindwing root stiffness was estimated as  $2.1e^{-4}Nm^2$  while the leading edge stiffness as  $7.8e^{-7}Nm^2$ , which is also within the range of the real hindwing.

### Wing Kinematics

In this study, the wing kinematics is the same as in the study of Young et al. [17] which is derived from Sun & Lan [14]. The pivot is assumed to be at  $0.75mm$ , which is approximately  $0.1\bar{c}_f$  from the wing root, while the pitching axis is placed at  $1.5mm$  (about  $0.2\bar{c}_f$ ) from the leading edge (Figure 1).

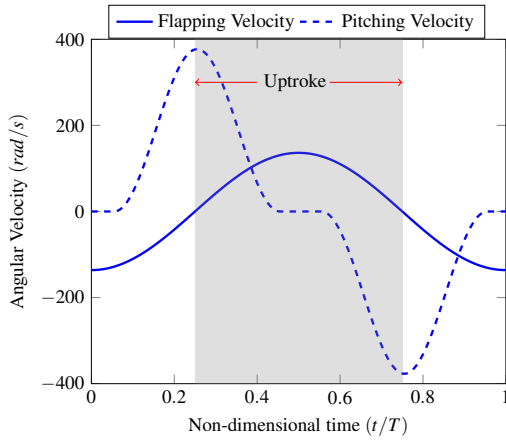


Figure 2. Wing kinematics of dragonfly [17]

The wing undergoes a sinusoidal flapping and pitching motion Figure 2, about the pivot point and pitching axis respectively. The wing flaps in a stroke plane inclined at  $52^\circ$  ( $\beta$ ) w.r.t the horizontal plane, with a flapping amplitude ( $\phi_0$ ) and frequency ( $f$ ) of  $34.5^\circ$  and  $36Hz$ , respectively.

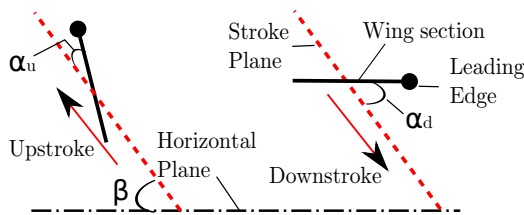


Figure 3. Schematic of wing kinematics.

The pitch amplitude taken is  $60^\circ$  and the pitch angle is defined with reference to the stroke plane. Figure 3 shows the schematic

of the wing section in mid-downstroke and mid-upstroke position. In the mid-downstroke, the wing is oriented horizontally with a pitch angle of  $52^\circ$  ( $\alpha_d$ ) while in the mid-upstroke it is nearly vertical with a pitch angle of  $8^\circ$  ( $\alpha_u$ ). These pitch angles are maintained for a brief period, before the wing starts supination or pronation.

### Computational Method & Validation

The *two-way* FSI simulations in this work were carried out using the commercial software ANSYS<sup>®</sup> 14.5. The fluid solver used was ANSYS FLUENT and the transient structural solver was ANSYS MECHANICAL. The fluid and the structural solvers exchange information between each other through the ANSYS SYSTEM COUPLING; an *implicit* coupling software which facilitates information exchange between the two solvers for several iterations within a single time step, before proceeding to the next one.

The FSI approach is validated against the computations of Gluck et. al[5]. Figure 4 shows the schematic of the test case, in which a 2D plate with a height and width of  $1m$  and  $0.06m$  respectively, is fixed at the bottom and is placed in a fluid domain. The plate is subjected to an initial pressure of  $100Pa$  on the left side for  $0.5s$ , which deflects the plate towards the right. After  $0.5s$ , the pressure is released and the plate tries to regain its mean position due to its elasticity and begins to oscillate. This oscillatory motion is dampened by the surrounding fluid and amplitude of oscillation gradually decreases over time.

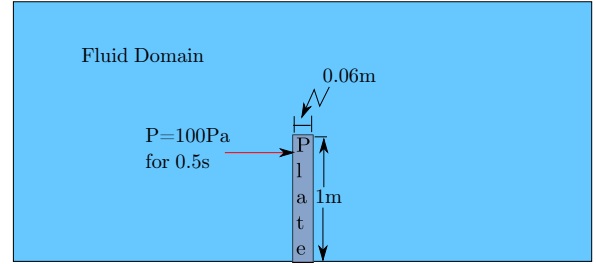


Figure 4. Validation Case Schematic[5].

The plate material has a density of  $2250kg/m^3$ , along with the Young's modulus and Poisson's ratio of  $2.5MPa$  and  $0.35$ , respectively. For the structural mesh, a 20 nodes brick element SOLID186 with quadratic shape function is used. The fluid has density of  $1kg/m^3$  and dynamic viscosity of  $0.2Pa \cdot s$ . The fluid domain is discretised with 1.18 million tetrahedral cells with the maximum mesh size of  $0.005m$  on the plate surface. The flow is assumed to be laminar and is simulated by solving the unsteady incompressible continuity and Navier Stokes equations, using FLUENT. The pressure and velocity were linked using the Semi-Implicit Pressure Linked equations (SIMPLE) and second order spatial discretisation was used. The plate displacement causes the surrounding fluid cells to deform. Based on the cell quality and cell size, certain cells are selected for remeshing and / or smoothing. This remeshing however, restricts the code to first order in time, in the current version. The simulation was carried out for a total time of  $50s$  with at time step size of  $0.05s$ . Figure 5 shows the deflection of the plate tip predicted by the FSI simulation and it is in agreement with that of Gluck et. al[5].

### Grid & Time-step Independence Study

This study was carried out on the rigid tandem wings. The computational domain and fluid mesh was generated in ANSA<sup>®</sup>, while FLUENT was used for the rigid wing simulations. The flow was assumed to be laminar and the fluid solver numeri-

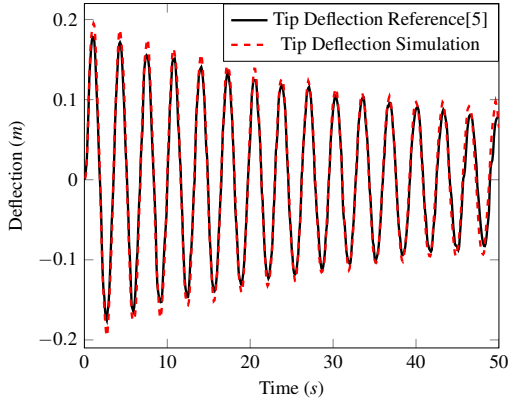


Figure 5. FSI Validation with simulation based reference[5]

cal schemes were the same as used in the validation case. Table 2 shows the mean lift coefficient ( $\bar{C}_l$ ) and mean drag coefficient ( $\bar{C}_d$ ) of the forewing for different grid and time step sizes. The first grid with maximum surface mesh size on the wings of  $0.018\bar{c}_f$  was chosen. This resulted in 85092 and 106702 cells on the fore and the hindwing respectively and a total volume mesh size of 4.5 million cells. This grid was tested at three time step sizes of  $T/500$ ,  $T/1000$  and  $T/2000$ , which showed very little variation in the forces and moments for both wings. To test grid independence, a second grid with maximum surface mesh size on the wings of  $0.012\bar{c}_f$  was chosen which resulted in nearly twice the number of cells on the fore and the hindwing (190316 & 239906) and a total volume mesh size of 7.4 million cells. The second grid was run with a time step size of  $T/1000$  and this showed less than 2% variation in the results. Similar results were observed for the hindwing. Finally, the first grid with  $T/1000$  was chosen for both rigid and flexible case to avoid negative volumes in the remeshing of the tetrahedral cells.

Case	Grid	Time-step	Forewing $\bar{C}_l$	Forewing $\bar{C}_d$
1	Coarse	$T/500$	0.3545	0.0019
2	Coarse	$T/1000$	0.3354	0.0027
3	Coarse	$T/2000$	0.3360	0.0036
4	Fine	$T/1000$	0.3354	0.003

Table 2. Grid and Time-step Independence Study.

## Results

The mean lift and drag coefficient of the rigid and flexible tandem wings are summarised in Table 3. In all the wings, the lift force is the dominant force as compared to the drag force which is nearly an order less in magnitude.

Wing	Type	$\bar{C}_l$	$\bar{C}_d$
Forewing	Rigid	0.3354	0.0027
Hindwing	Rigid	0.2371	0.0367
Forewing	Flexible	0.3716	$2e^{-4}$
Hindwing	Flexible	0.2784	0.042

Table 3. Summary of tandem wings results.

The lift coefficient time history of the tandem forewing and hindwing is shown in Figure 6 and Figure 7, respectively. The flexible forewing has a lower positive and negative lift peak as compared to the rigid forewing. But overall, the flexible forewing generates nearly 10% higher lift than the rigid counterpart. In the flexible hindwing, the positive lift peak is significantly higher than the rigid hindwing and it generates nearly

17% higher mean lift.

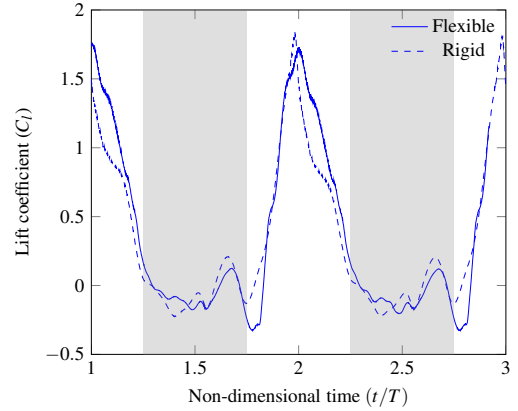


Figure 6. Tandem forewing lift coefficient.

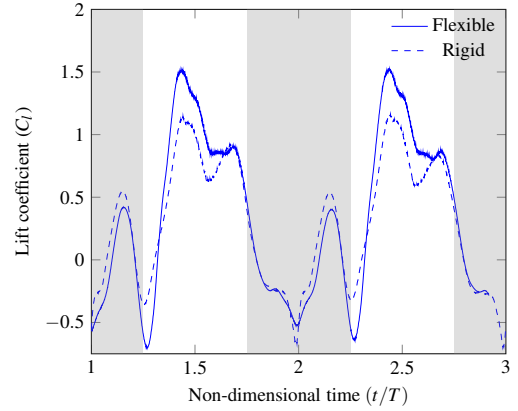


Figure 7. Tandem hindwing lift coefficient.

We analyse the flow fields at  $t/T = 2.45$ , when both the hindwings reach close to their respective lift peaks. From the schematic of the positions of the flexible and rigid hindwing at  $t/T = 2.45$  in Figure 8, it is clear that the flexible hindwing shows a significant deflection from the midspan to the wing tip. Both wings are approaching the mid-downstroke position and have developed a LEV and TV by this stage (Figure 9), however these vortices are stronger in the flexible hindwing. The upper surface of the flexible hindwing hence shows larger and stronger negative pressure zone accompanied by a relatively higher positive pressure below the wing surface (Figure 10), resulting in a significant gain in lift as compared to the rigid hindwing.

In summary, wing flexibility has enhanced the lift generated by both wings. However, the performance of the flexible forewing and hindwing in tandem as compared to single flexible counterparts need to be explored. In a computational study on dragonfly hover flight at phase  $180^\circ$  using rigid wings, Sun & Lan [14] found that the forewing and the hindwing produced 14% and 16% less lift in tandem arrangement, as they did when they flapped as a single wing. Other studies [7, 10, 15] using rigid wings, found a similar reduction in the lift generated by each tandem wings, in most phases. It would be interesting to investigate whether the performance is similar for flexible tandem wings.

## Conclusions

Flexibility in tandem wings produces a gain of lift in both the forewing (10%) and the hindwing (17%) as compared to the

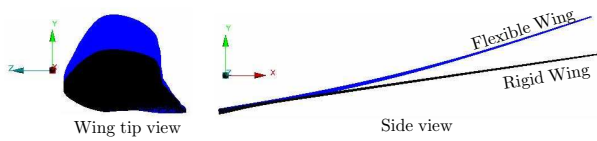


Figure 8. Tandem hindwing position at  $t/T = 2.45$ .

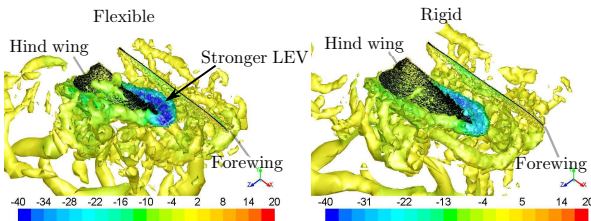


Figure 9. Vortical structures (using Q-criterion) superimposed with pressure [-40 to 20Pa] at  $t/T = 2.45$ .

rigid tandem wings. The higher and lower lift peaks in the flexible forewing are nearly the same as that of the rigid forewing. The positive lift peak of the flexible hindwing near the mid-downstroke position is significantly higher than that of the rigid one. At this position, the flexible hindwing shows significant spanwise bending with a stronger LEV on the upper surface and higher pressure at the bottom, augmenting the lift force.

#### Acknowledgements

The work is conducted in part with a grant under the Merit Allocation scheme of the National Facility of the National Computational Infrastructure. The first author would like to thank the team at ANSA<sup>®</sup> for their support.

#### References

- [1] Alexander, D. E., Unusual phase relationships between the forewing and hindwings in flying dragonflies, *Journal of Experimental Biology*, **109**, 1984, 379–383.
- [2] Alexander, D. E., Wind tunnel studies of turns by flying dragonflies, *Journal of Experimental Biology*, **122**, 1985, 81–98.
- [3] Chen, J.-S., Chen, J.-Y. and Chou, Y.-F., On the natural frequencies and mode shapes of dragonfly wings, *Journal of Sound and Vibration*, **313**, 2008, 643–654.
- [4] Combes, S. A. and Daniel, T. L., Flexural stiffness in insect wings ii. spatial distribution and dynamic wing bending, *Journal of Experimental Biology*, **206**, 2003, 2989–2997.
- [5] Glück, M., Breuer, M., Durst, F., Halfmann, A. and Rank, E., Computation of fluid–structure interaction on lightweight structures, *Journal of Wind Engineering and Industrial Aerodynamics*, **89**, 2001, 1351–1368.
- [6] Hamamoto, M., Ohta, Y., Hara, K. and Hisada, T., Application of fluid–structure interaction analysis to the flapping flight of insects with deformable wings., *Advanced Robotics*, **21**, 2007, 1–21.
- [7] Hu, Z., McCauley, R., Schaeffer, S. and Deng, X., Aerodynamics of dragonfly flight and robotic design, *IEEE International Conference on Robotics and Automation*.

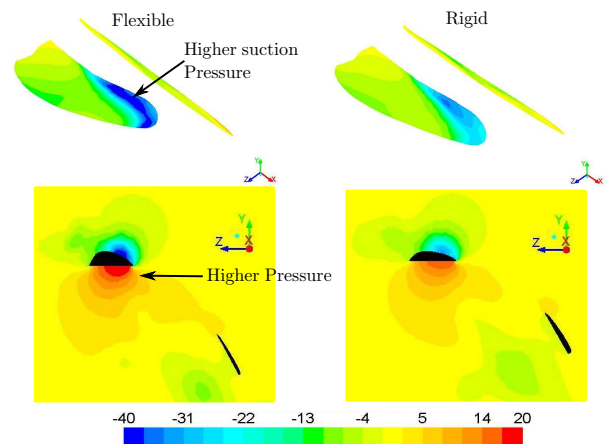


Figure 10. Pressure [-40 to 20Pa] on wing surface (top) & 75% plane section (bottom) at  $t/T = 2.45$ .

- [8] Lehmann, F. O., Wing-wake interaction reduces power consumption in insects tandem wings., *Experiments of Fluids*, **46**, 2009, 765–775.
- [9] Maybury, W. J. and Lehmann, F.-O., The fluid dynamics of flight control by kinematic phase lag variation between two robotic insect wings., *Journal of Experimental Biology*, **207**, 2004, 4707–4726.
- [10] Nagai, H., Isogai, K. and Fujimoto, T., Experimental study on flow interaction between fore and hindwings of dragonfly in hovering and forward flight, *International Congress of the Aeronautical Sciences*.
- [11] Norberg, R. A., The pterostigma of insect wings an inertial regulator of wing pitch, *Journal of Comparative Physiology*, **81**, 1972, 9–22.
- [12] Okamoto, M., Yasuda, K. and Azuma, A., Aerodynamic characteristics of the wings and body of a dragonfly, *Journal of experimental biology*, **199**, 1996, 281–294.
- [13] Sane, S. P., The aerodynamics of insect flight, *Journal of Experimental Biology*, **206**, 2003, 4191–4208.
- [14] Sun, M. and Lan, S. L., A computational study of the aerodynamic forces and power requirements of dragonfly (*aeschna juncea*) hovering, *Journal of Experimental Biology*, **207**, 2004, 1887–1901.
- [15] Wang, J. K. and Sun, M., A computational study of the aerodynamics and forewing–hindwing interaction of a model dragonfly in forward flight, *Journal of Experimental Biology*, **208**, 2005, 3785–3804.
- [16] Yamamoto, M. and Isogai, K., Measurement of unsteady fluid dynamic forces for a mechanical dragonfly model, *AIAA Journal*, **43**, 2005, 2475–2480.
- [17] Young, J., Lai, J. C. and Germain, C., Simulation and parameter variation of flapping-wing motion based on dragonfly hovering, *AIAA Journal*, **46**, 2008, 918–924.
- [18] Young, J., Walker, S. M., Bomphrey, R. J., Taylor, G. K. and Thomas, A. L. R., Details of insect wing design and deformation enhance aerodynamic function and flight efficiency, *Science*, **325**, 2009, 1549–1552.